Wavelength-dependent scattering in spectroscopic optical coherence tomography

Chenyang Xu, P. Scott Carney, and Stephen A. Boppart

Biophotonics Imaging Laboratory, Beckman Institute for Advanced Science and Technology, Department of Electrical and Computer Engineering, University of Illinois at Urbana-Champaign, 405 N Mathews Ave., Urbana, IL 61801
boppart@uiuc.edu

Abstract: The particle sizing capabilities of light scattering spectroscopy (LSS) and the spatial localization of optical coherence tomography (OCT) are brought together in a new modality known as scattering-mode spectroscopic OCT. An analysis is presented of the spectral dependence of the light collected in spectroscopic OCT for samples comprised of spherical particles. Many factors are considered including the effects of scatterer size, interference between the fields scattered from closely adjacent scatterers, and the numerical aperture of the OCT system. The modulation of the spectrum of the incident light by scattering of a plane wave from a single sphere is a good indicator of particle size and composition. However, it is shown in this work that the sharp focusing of fields causes the spectral signature to shift and the presence of multiple scatterers has dramatic modulation effects on the spectra. Approaches for accurately matching physical structure with the observed signals under various conditions are discussed.

OCIS codes: (110.4500) Optical coherence tomography; (290.0290) Scattering; (300.0300) Spectroscopy

References and links

1. A. Ben-Reuven and N.D. Gershon, "Light scattering by orientational fluctuations in liquids," J. Chem. Phys. **51,** 893-902 (1969).
2. S.R. Aragon and E. Pecora, "Theory of dynamic light scattering from large anisotropic particles," J. Chem. Phys. **66,** 2506-2516 (1977).
3. L.T. Perelman, V. Backman, M. Wallace, G. Zonios, R. Manoharan, A. Nusrat, S. Schields, M. Seiler, C. Lima, T. Hamano, I. Itzkan, J. Van Dam, J.M. Crawford, and M.S. Feld, "Observation of periodic fine structure in reflectance from biological tissue: A new technique for measuring nuclear size distribution," Phys. Rev. Lett. **80,** 627-630 (1998).
4. V. Backman, M.B. Wallace, L.T. Perelman, J.T. Arendt, R. Gurjar, M.G. Muller, Q. Zhang, G. Zonios, E. Kline, T. Mcgillican, S. Shapshay, T. Valdez, K. Badizadegan, J.M. Crawford, M. Fitzmaurice, S. Kabani, H.S. Levin, M. Seiler, R.R. Dasari, I. Itzkan, J. Van Dam, and M.S. Feld, "Detection of preinvasive cancer cells," Nature **406,** 35-36 (2000).
5. N.N. Boustany, S.C. Kuo, and N.V. Thakor, "Optical scatter imaging: subcellular morphometry in situ with Fourier filtering," Opt. Lett. **26,** 1063-1065 (2001).
6. J.R. Mourant, "Spectroscopic diagnosis of bladder cancer with elastic light scattering," Laser Surgical Medicine **17,** 350-357 (1995).
7. C. Yang, L.T. Perelman, A. Wax, R.R. Dasari, and M.S. Feld, "Feasibility of field-based light scattering spectroscopy," J. Biomed. Opt. **5,** 138-143 (2000).
8. A. Wax, C. Yang, and J.A. Izatt, "Fourier-domain low-coherence interferometry for light-scattering spectroscopy," Opt. Lett. **28,** 1230-1232 (2003).
9. J.W. Pyhtila, R.N. Graf, and A. Wax, "Determining nuclear morphology using an improved angle-resolved low coherence interferometry system," Opt. Express **11,** 3473-3484 (2003).
10. J.W. Pyhtila and A. Wax, "Rapid, depth-resolved light scattering measurements using Fourier domain, angle-resolved low coherence interferometry," Opt. Express **12,** 6178-6183 (2004).

#7680 - $15.00 USD Received 2 June 2005; revised 26 June 2005; accepted 29 June 2005

11. D. Huang, E.A. Swanson, C.P. Lin, J.S. Schuman, W.G. Stinson, W. Chang, M.R. Hee, T. Flotte, K. Gregory, C.A. Puliafito, and J.G. Fujimoto, "Optical coherence tomography," Science **254,** 1178-1181 (1991).
12. A.F. Fercher, W. Drexler, C.K. Hitzenberger, and T. Lasser, "Optical coherence tomography - principles and applications," Rep. Prog. Phys. **66,** 239-303 (2003).
13. U. Morgner, W. Drexler, F.C. Kartner, X.D. Li, C. Pitris, E.P. Ippen, and J.G. Fujimoto, "Spectroscopic optical coherence tomography," Opt. Lett. **25,** 111-113 (2000).
14. R. Leitgeb, M. Wojtkowski, A. Kowalczyk, C.K. Hitzenberger, M. Sticker, and A.F. Fercher, "Spectral measurement of absorption by spectroscopic frequency-domain optical coherence tomography," Opt. Lett. **25,** 820-822 (2000).
15. D.J. Faber, E.G. Mik, M.C.G. Aalders, and L.T.G. V., "Light absorption of (oxy-)hemoglobin assessed by spectroscopic optical coherence tomography," Opt. Lett. **28,** 1436-1438 (2003).
16. C. Xu, J. Ye, D.L. Marks, and S.A. Boppart, "Near-infrared dyes as contrast-enhancing agents for spectroscopic optical coherence tomography," Opt. Lett. **29,** 1647-1649 (2004).
17. B. Hermann, K. Bizheva, A. Unterhuber, B. Povazay, H. Sattmann, L. Schmetterer, A.F. Fercher, and W. Drexler, "Precision of extracting absorption profiles from weakly scattering media with spectroscopic time-domain optical coherence tomography," Opt. Express **12,** 1677-1688 (2004).
18. R. Gurjar, V. Backman, J.M. Peralta, I. Georgakoudi, K. Badizadegan, I. Itzkan, R.R. Dasari, and M.S. Feld, "Imaging human epithelial properties with polarized light-scattering spectroscopy," Nature Medicine **7,** 1245-1248 (2001).
19. T.H. Ko, D.C. Adler, J.G. Fujimoto, D. Mamedov, V. Prokhorov, V. Shidlovski, and S. Yakubovich, "Ultrahigh resolution optical coherence tomography imaging with a broadband superluminescent diode light source," Opt. Express **12,** 2112-2119 (2004).
20. A. Dubois, G. Moneron, K. Grieve, and A.C. Boccara, "Three-dimensional cellular-level imaging using full-field optical coherence tomography," Phys. Med. and Biol. **49,** 1227-1234 (2004).
21. C. Xu, F. Kamalabadi, and S.A. Boppart, "Comparative performance analysis of time-frequency distributions for spectroscopic optical coherence tomography," Appl. Opt. **44,** 1813-1822 (2005).
22. C. Xu, D.L. Marks, M.N. Do, and S.A. Boppart, "Separation of absorption and scattering profiles in spectroscopic optical coherence tomography using a least-squares algorithm," Opt. Express **12,** 4790-4803 (2004).
23. P.S. Carney, V.A. Markel, and J.C. Schotland, "Near-field tomography without phase retrieval," Phys. Rev. Lett. **86,** 5874-5877 (2001).
24. A. Wax, C. Yang, V. Backman, K. Badizadegan, C.W. Boone, R.R. Dasari, and M.S. Feld, "Cell organization and substructure measured using angle-resolved low coherence interferometry," Biophys. J. **82,** 2256-2264 (2002).
25. D.C. Adler, T.H. Ko, P.R. Herz, and J.G. Fujimoto, "Optical coherenece tomography contrast enhancement using spectroscopic analysis with spectral autocorrelation," Opt. Express **12,** 5487-5501 (2004).
26. J.M. Schmitt, S.H. Xiang, and K.M. Yung, "Speckle in optical coherence tomography," J. Biomed. Opt. **4,** 95-105 (1999).

1. Introduction

Light scattering spectroscopy (LSS) is a method used extensively for measuring particle sizes [1,2]. In the last decade, there has been a growing interest in applying LSS techniques to *in vivo* biological tissue in order to obtain structural and functional data. Particularly, light scattering has been used to measure the size distribution of cell nuclei and mitochondria, which can be altered in cancerous or pre-cancerous cells [3-6]. In these studies, the intensity of the white light scattering from tissue is measured via an optical probe and either the spectrum or the angular distribution of this light is analyzed. The cells, nuclei, or cellular organelles are assumed to be Mie scatterers, and the experimental data are fit to the existing model to retrieve size or refractive index information. Recently, LSS has been implemented with low-coherence interferometry (LCI), which offers the possibility of depth-resolved analysis of the LSS signal [7-10]. However, there remain three important limiting factors in the LSS studies to date. First, because the LSS typically utilizes collimated beams or focusing lenses with very low numerical aperture (NA), there usually is very poor lateral resolution. Second, the collected back-scattered signal intensity in LSS is low because the collection efficiency is proportional to the NA of the focusing lens. Third, the penetration depth of LSS is quite limited due to the effect of multiple-scattering (for non-LCI-based LSS). Because of these shortcomings, LSS, to date, has primarily been used as a functional *analysis* method rather than a functional *imaging* method.

#7680 - $15.00 USD Received 2 June 2005; revised 26 June 2005; accepted 29 June 2005

Optical coherence tomography (OCT) is an LCI-based technique for biomedical imaging. OCT typically utilizes high a NA lens to achieve high lateral resolutions between 1-10 μm [11,12]. Because OCT utilizes heterodyne detection and broadband coherence gating, the OCT signal is mostly due to single scattering events within the coherence gate. Therefore, current state-of-the-art OCT systems have deep penetration (1-2 mm in typical tissue) and 1-3 μm depth resolution. A recent functional extension of OCT, called spectroscopic OCT (SOCT), allows the spectroscopic information of back-scattered light to be analyzed in a depth-resolved way [13,14]. SOCT has undergone rapid development recently, both in theory and methodology, with many possible applications [15-17]. However, to date, most SOCT studies have focused on imaging the wavelength-dependent absorption from either endogenous or exogenous absorbers. Because the absorption of light takes place over the entire optical path that the OCT probe field traverses, while the scattering takes place at the local interfaces of refractive index inhomogeneities, measuring the wavelength-dependent scattering could be a more sensitive and localized indicator, compared to measuring the wavelength-dependent absorption. Therefore in this paper, we develop the theory, methodology, and applications of SOCT based on spectral scattering.

A combination of LSS techniques with SOCT techniques to form a new functional imaging method, that we call scattering-mode SOCT, offers many advantages. LSS is a technique with more than 50 years of history, extensive literature, and algorithms that can be readily used for many applications. The recently-developed SOCT offers a method for acquiring LSS signal with 3D spatial resolution. In addition, by coherence gating, SOCT helps to distinguish the single-scattering components from the diffusive scattering background, which at present is accomplished by polarization gating [18]. For scatterers that are large compared to the central wavelength, such as for cell nuclei, the scatterer size can be measured directly by OCT if high NA optics are used. In this scenario, scattering-mode SOCT is still valuable for measuring the refractive index of the scatterers. For scatterers with size comparable to the imaging wavelength or even smaller (such as subcellular organelles like mitochondria), it is typically impossible to accurately distinguish the exact size of the scatterer by standard OCT imaging. However, the scatterer size could be estimated by LSS. Thus, in principle, small scatterer sizes could also be estimated by scattering-mode SOCT in a depth-resolved fashion. To date, the use of SOCT for accurately measuring wavelength-dependent scattering has not been shown. We believe that this problem is complicated by the following factors:

1. The broadband light sources commonly used in OCT systems span a relatively narrow wavelength range compared to the thermal light sources used in LSS setups.
2. SOCT suffers from a time-frequency analysis tradeoff. Therefore, the spectral resolution is limited in SOCT for a given spatial resolution. This is not a problem for LSS because the spatial resolution is either very poor or not even considered in LSS.
3. There are two major SOCT spectral modification mechanisms in the tissue: the wavelength-dependent attenuation by the media before the coherence gate and the wavelength-dependent scattering by the scatterers within the coherence gate. This is not a problem for LSS because in traditional LSS only shallow structures are imaged and it is assumed that tissues are homogeneous.
4. SOCT typically uses a tightly-focused beam, which can not be simply treated as collimated plane waves incident on the tissue, as often assumed in LSS.
5. There may be multiple but not an infinite number of scatterers within the imaging volume defined by both the coherence gating and the imaging beam profile, causing speckle patterns as a result of spectral interference. In LSS, the imaging volume typically is much larger, such that the spectral interference tends to be averaged out spatially.

With the rapid development of ultra-broadband laser technology in the last five years, the available OCT laser bandwidth has increased dramatically, and is expected to continue to increase. Therefore, the first factor above is expected to be solved soon, especially with the development of multiplexed laser sources and the recent use of thermal light sources in OCT

#7680 - $15.00 USD Received 2 June 2005; revised 26 June 2005; accepted 29 June 2005

technology [19,20]. The second and the third factors are signal-processing problems. The optimal spectral analysis methods for SOCT signal are not conventional linear spectral analysis methods, but joint time-frequency analysis methods [21]. In addition, the time-frequency analysis and the experimental data retrieval should be integrated together. Spectral cues and spatial cues can be utilized to separate the contribution of different spectral modification processes [22]. In this paper, the effect of tightly-focused beams and the spectral modulation due to multiple-scatterers in the imaging volume will be discussed. In Section 2.1 a method to study the effects of tightly focused beams is presented by decomposing the incident Gaussian beam into plane wave components, and coherently summing up the scattering contribution from each plane wave. In Section 2.2 a method for studying the effects of multiple-scatterers in the imaging volume is presented based on the coherent summation of scattering from a single scatterer formulated in Section 2.1. In Section 3 the numerical simulations are presented and conclusions based on the simulation results are drawn. In Section 4 the approaches for accurately matching physical structure with the observed signals under various conditions are discussed.

2. Theory:

2.1 Beam effects in a single scattering event

The refractive-index inhomogeneities in tissue are treated as discreet scattering particles. It is assumed that the individual features may be strongly scattering, and that the single particle scattered field may need to be computed non-perturbatively. However, it is further assumed that the field arising from inter-particle scattering will be weak, will tend to acquire a longer delay, and so will fall outside the coherence gate of the OCT system. Here, when the inter-particle scattering is ignored, the resultant field is said to arise from single-scattering. This is not single-scattering in the sense of the Born series, but may be obtained from a perturbative calculation keeping the lowest order in the particle density. In general, for a single scattering event in OCT, the collected scattered field is dependent on the properties of the incident light, the focusing lens, the position of the scatterer in the beam, and the properties of the scatterer (Fig. 1).

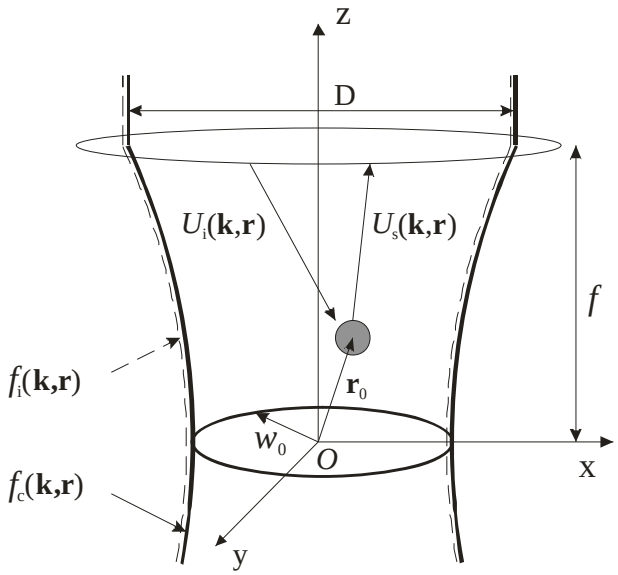

Fig. 1. Diagram of wavelength-dependent single-scattering from a Gaussian beam, where $\mathbf{r}_0$ is the position of the scatterer relative to the center of the Gaussian beam at the waist. The functions $f_i(\mathbf{k},\mathbf{r})$ and $f_c(\mathbf{k},\mathbf{r})$ describe the incident and collection Gaussian modes, respectively, D is the beam diameter incident on the lens, and f is the focus length of the achromatic lens.

#7680 - $15.00 USD Received 2 June 2005; revised 26 June 2005; accepted 29 June 2005

Because OCT typically uses single-mode Gaussian beam illumination and an achromatic lens, the illumination mode for a specific optical frequency at the beam waist is a Gaussian function with constant phase,

$$f_i(x, y, k_0) = \frac{1}{w_0(k_0)} \exp\left[-\frac{x^2 + y^2}{w_0^2(k_0)}\right], \tag{1}$$

where $k_0 = 2\pi / \lambda_0$ is the free-space wavenumber and $w_0(k_0)$ is the Gaussian beam waist radius. These relations assume that the chosen coordinate system is centered on the beam waist (see Fig. 1). If an achromatic lens of focal length f is used, the $w_0(k_0)$ is wavelength dependent:

$$w_0(k_0) = \frac{4f}{k_0 D}. \tag{2}$$

In order to make use of the existing scattering theory for plane-wave incident fields, the Gaussian beam in Eq. (1) is decomposed into its transverse Fourier components in the waist plane,

$$F_i(\mathbf{q}_i, k_0) = \tfrac{1}{2} w_0(k_0) \exp\left[-\frac{w_0^2(k_0)}{4} q_i^2\right], \tag{3}$$

where $\mathbf{q}_i$ are the transverse spatial frequencies of the incident beam, $\mathbf{q}_i = k_{i,x}\hat{x} + k_{i,y}\hat{y}$. It should be noted there are considerably higher amplitudes for higher transverse spatial frequencies in OCT than in conventional LSS because tightly-focusing high NA lenses are used in OCT.

Taking $C^2(k_0)$ to be the spectrum of the light source, the angular spectrum of illuminating field $U_i(\mathbf{q}_i, k_0)$ is:

$$U_i(\mathbf{q}_i, k_0) = C(k_0) F_i(\mathbf{q}_i, k_0) = \tfrac{1}{2} C(k_0) w_0(k_0) \exp\left[-\frac{w_0^2(k_0)}{4} q_i^2\right]. \tag{4}$$

The field of transverse spatial frequency $\mathbf{q}_s$ scattered from the scatterer is the integral of the scattered field arising from all incident transverse spatial frequencies:

$$U_s(\mathbf{q}_s, k_0) = \int C(k_0) F_i(\mathbf{q}_i, k_0) e^{i[\mathbf{r}_0 \bullet (\mathbf{k}_i - \mathbf{k}_s)]} R(\mathbf{q}_i, \mathbf{q}_s, k_0, P)\, d^2 q_i \ , \tag{5}$$

where $\mathbf{r_0}$ denotes the spatial position of the scatterer. P represents properties of the scatterer (*e.g.*, size, refractive index, etc.). $R(\mathbf{q}_i, \mathbf{q}_s, k_0, P)$ is the function that relates the incident plane wave of transverse spatial frequency $\mathbf{q}_i$ to the scattered plane wave of transverse spatial frequency $\mathbf{q}_s$ when the scatterer is located at the origin. In general, $R(\mathbf{q}_i, \mathbf{q}_s, k_0, P)$ can only be found by numerical methods. However, for homogeneous dielectric spheres with radius a and refractive index n, and ignoring the polarization effects and sphere to sphere scattering, R has an analytic solution [23]:

$$R(\mathbf{q}_i, \mathbf{q}_s, k_0, P) = \sum_{l=0}^{\infty} A_l P_l\left(\frac{\mathbf{k}_i \cdot \mathbf{k}_s}{k_0^2}\right), \tag{6}$$

where $\mathbf{k}_i, \mathbf{k}_s$ are the 3D spatial frequencies, $\mathbf{k} = \mathbf{q} + k_z \hat{z}$. For any given $\mathbf{q}$, the $\mathbf{k}$ can be calculated by the dispersion relationship $q^2 + k_z^2 = k_0^2$. A_l are the usual partial wave expansion coefficients and P_l are the Legendre polynomials:

#7680 - $15.00 USD Received 2 June 2005; revised 26 June 2005; accepted 29 June 2005

$$
\begin{aligned}
A_l &= \frac{i\beta_l}{k_0(\beta_l - i\gamma_l)}, \\
\beta_l &= j_l(nk_0a)\,j_l'(k_0a) - nj_l'(nk_0a)\,j_l(k_0a), \\
\gamma_l &= nj_l'(nk_0a)\,n_l(k_0a) - j_l(nk_0a)\,n_l'(k_0a).
\end{aligned} \tag{7}
$$

The $j_l(x)$, $n_l(x)$, $j_l'(x)$ and $n_l'(x)$ are spherical Bessel functions of the first and second kind, with their respective derivatives.

The field coupled back into the lens $S(k_0,P)$, is the sample-arm field for the OCT interferometer. $S(k_0,P)$ is calculated by integrating the secondary sources over the collection beam profile $F_c(\mathbf{q}_s,k_0)$.

$$
\begin{aligned}
S(k_0,P) &= \int U_s(\mathbf{q}_s,k_0)F_c(\mathbf{q}_s,k_0) \\
&= \iint C(k_0)F_i(\mathbf{q}_i,k_0)e^{i[\mathbf{r}_0\bullet(\mathbf{k}_i-\mathbf{k}_s)]}R(\mathbf{q}_i,\mathbf{q}_s,k_0,P)F_c(\mathbf{q}_s,k_0)d^2q_i d^2q_s\ .
\end{aligned} \tag{8}
$$

Different from LSS, where separate illumination and collection optics are used, OCT uses the same set of optics for illumination and collection. Therefore, Eq. (8) can be simplified as:

$$
S(k_0,P) = \iint C(k_0)F_i(\mathbf{q}_i,k_0)e^{i[\mathbf{r}_0\bullet(\mathbf{k}_i-\mathbf{k}_s)]}R(\mathbf{q}_i,\mathbf{q}_s,k_0,P)F_i^*(\mathbf{q}_s,k_0)d^2q_i d^2q_s\ . \tag{9}
$$

Eq. (9) shows that the scattering in a tightly focused beam is dependent on the beam parameters, the properties of the scatterers, and the location of the scatterers. In the frequency domain, the measured OCT cross-correlation signal is

$$
I(k_0,P) = S(k_0,P)|U_R(k_0)|\exp[i\phi(k_0)], \tag{10}
$$

where $U_R(k_0)$ is the field returning from the reference arm. The quantity $\phi(k_0)$ is the phase difference between the sample and reference arms. If a perfect mirror is used in the reference arm, the reference spectrum is the same as the optical source spectrum $C(k_0)$. For most practical systems, there are phase variations that are difficult to accurately measure, however, the intensity of $I(k_0,P)$ can be measured quite reliably. Therefore, in the following simulations, only the intensity of the signal is considered, *i.e.*,

$$
|I(k_0,P)| = |C(k_0)||S(k_0,P)|. \tag{11}
$$

2.2. Effect of multiple scatterers in the SOCT imaging volume

The imaging volume represented by a voxel in a standard OCT image is defined by the Gaussian beam width and the coherence gating, centered at the nominal voxel position. The voxel intensity is a coherent sum of scattering from all scatterers inside the imaging volume. In SOCT, due to the time-frequency uncertainty principle, in order to achieve reasonable spectral resolution, the imaging volume is usually considerably larger than in standard OCT. The imaging volume in SOCT is defined by the Gaussian beam width and the coherence gating of a particular spectral sub-band (or the time window length if the STFT is used). Although the imaging volume in SOCT is larger than in standard OCT, the single scattering approximation still holds for most cases.

Let the time window in SOCT be described by a spatially dependent function $h(z)$. Assuming all single-scattering events, the collected OCT signal intensity from N scatterers inside an imaging volume in the spectral domain is,

$$
|I(k_0)| = |C(k_0)|\left|H(k_0) * \sum\nolimits_{n=1}^{N} S_n(k_0,P_n)\right|, \tag{12}
$$

where H is the Fourier transform of the window h.

#7680 - $15.00 USD Received 2 June 2005; revised 26 June 2005; accepted 29 June 2005

Using Eq. (9),

$$\sum_{n=1}^{N} S_n(k_0, P_n) = \sum_{n=1}^{N} \iint C(k_0) F_i(\mathbf{q}_i) F_i^*(\mathbf{q}_s) e^{i[\mathbf{r}_n \cdot (\mathbf{k}_i - \mathbf{k}_s)]} R(\mathbf{k}_i, \mathbf{k}_s, k_0, P_n) d^2 k_i d^2 k_s \text{ , (13)}$$

where $R(\mathbf{k}_i, \mathbf{k}_s, k_0, P_n)$ represents the wavelength-dependent scattering amplitude of the n-th scatterer located at the origin.

It may be seen from Eq. (12) and (13) that the scattering-mode SOCT signal will be obtained from a coherent superposition of the fields scattered from many plane waves and by many scatterers. In standard LSS, particle size is determined by observing the spectrum of the scattered field and matching the spectral signature to a particular particle size. It is evident here that the spectral interference arising from the coherent superposition given in Eq. (12) will make such a procedure complicated for scattering-mode SOCT. The measured OCT spectral intensity always has a modulation term that depends on the number and the positions of the scatterers. Therefore, algorithms need to be developed to jointly estimate the scatterer property and location. Through numerical studies, we identify two cases when solutions are readily available. When it is know *a priori* that the sample consists of practically identical particles, then one simple method is to average many incoherent SOCT measurements. In a sense, conventional LSS performs this incoherent averaging by using a large beam width and spatially-incoherent light sources. In a second less obvious case, when one expects only one large scatterer surrounded by many smaller scatterers within the SOCT voxel, then an over-sampling procedure will allow us to accurately estimate particle size.

3. Simulation

In order to understand the analytical results of the previous section, simulations were constructed to test the theory and to offer important insight into the scattering-mode SOCT. The tissue was modeled as a material with spheres of different sizes distributed over the volume of interest. Computations were done to obtain the normalized spectral scattering cross-sections and the total intensity distributions for spheres. Different parameters for the incident beams and the particle sizes and locations were used.

3.1. Effect of a focused Gaussian beam

The laser was assumed to have a perfect Gaussian spectrum centered at 800 nm and having a FWHM bandwidth of 200 nm. The Gaussian beam of different beam waists $w_0(k_0)$ was simulated according to Eq. (3), where the total beam intensity was normalized. An achromatic optical focusing system was assumed according to Eq. (2). For each $w_0(k_0)$, the 2D spatial frequencies were digitized by uniformly sampling an 11x11 frequency grid covering the $[-2/w_{0,800nm}, 2/w_{0,800nm}]$ space. The error of the total integrated intensity of such digitization compared to the perfect Gaussian beam was about 0.3%. The diameters of the spheres were chosen to mimic two types of biological scatterers: 8 μm for cell nuclei and 1.6 μm for cellular organelles such as mitochondria. The refractive indices of the spheres and the media were set to be 1.45 and 1.37, to mimic the refractive indices of nuclei and cytoplasm, respectively [24].

Figure 2 shows the normalized collected spectral signal for different beam parameters when single spheres are located at the center of the Gaussian beam. If the beam waist spot size $w_0(k_0)$ is large compared to wavelength, the scattering spectrum for both large spheres and small spheres are comparable to those for the plane wave scattering case. If the beam waist spot size $w_0(k_0)$ is small, or comparable to the wavelength, there are significant deviations. Particularly, it was found that if the total laser power is normalized, decreasing the beam waist spot size produces an increase in amplitude and a shift of the scattering spectrum. The shift is in the direction of decreasing wavelength. While this spectral shift obscures the frequency response of the large particles, it preserves some pattern for small particles.

#7680 - $15.00 USD Received 2 June 2005; revised 26 June 2005; accepted 29 June 2005

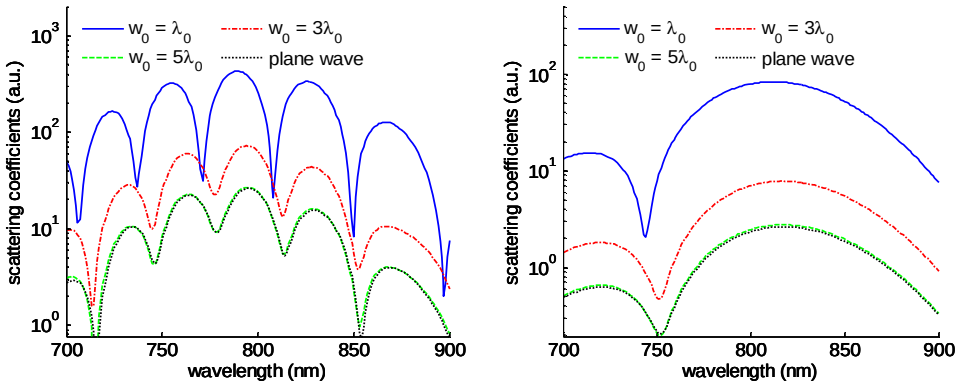

Fig. 2. Beam wavelength-dependent spectral patterns for (a) centered large spheres ($r = 5\lambda$) and (b) small spheres ($r = \lambda$). In each case, the incident laser beam has different beam waist sizes.

There are currently two approaches for sizing the scatterers based on the measured spectra. The first approach is based on pitch detection such as using the Fourier transform or determining the autocorrelation. The principle behind the first approach is that the oscillation "frequency" in the wavelength-dependent scattering is size dependent, such that larger scatterers tend to produce more oscillatory patterns [3]. The second approach is based on curve fitting such as using least-square or χ^2 methods [24]. The second approach provides an exhaustive search of possible scattering sizes and attempts to fit the normalized experimental measurement to the theoretical prediction. As can be seen from Fig. 2, there are significant spectral shifts in the case of small w_0 , but the oscillation pitch is largely preserved. Therefore, it is expected that for small w_0 , the first approach will be more appropriate for matching the measured wavelength-dependent scatterings to those calculated based on plane waves.

Figure 3 shows the normalized wavelength-dependent scattering of spheres that are in-focus, but located off-center in the Gaussian beam. For large beam waist sizes, a sphere

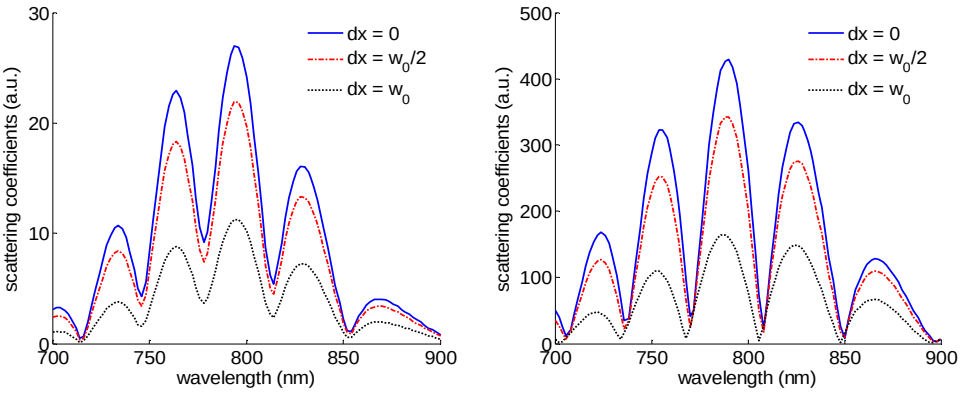

Fig. 3. Scattering spectral patterns for in-focus off-center spheres ($r = 5\lambda$) for different off-center positions and different beam waist sizes w_0 . (a): $w_0 = 5\lambda_0$; (b): $w_0 = \lambda_0$.

located off-center caused an almost proportional decrease in the magnitude compared to the original pattern. However, for small beam waist sizes, the wavelength-dependent scattering

#7680 - $15.00 USD Received 2 June 2005; revised 26 June 2005; accepted 29 June 2005

not only decreases in magnitude, but also shifts in wavelength. The shift in wavelength for off-center scatterers is in the direction of deceasing wavelength.

Figure 4 shows that if an off-center particle in the focal plane is moved out of the focal plane in the direction of the z axis (beam propagation axis), the resulting wavelength-dependent scattering effect is a decrease in the magnitude of the scattering pattern depending on the original position of the particle. However, except for chromatic dispersion effects, most of the scattering spectral shape is preserved. The chromatic dispersion causes a decrease of wavelength-dependent scattering amplitude for longer wavelengths. This decrease of power is due to the larger beam size at longer wavelengths.

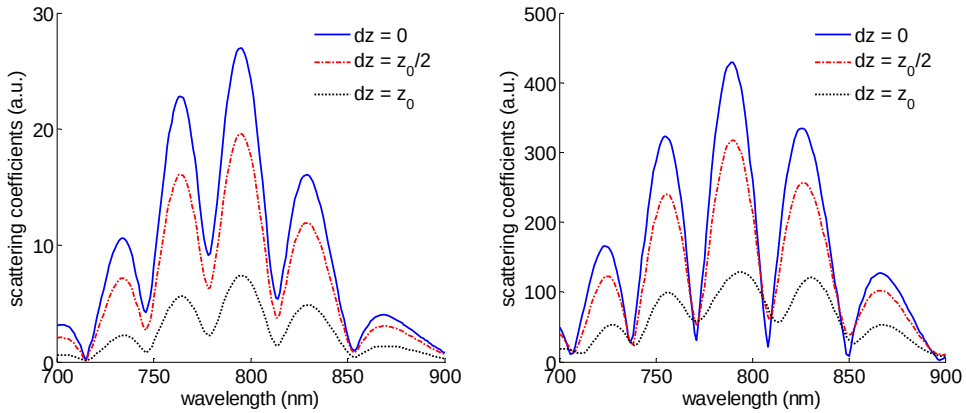

Fig. 4. Scattering spectral patterns for off-focus spheres ($r = 5\lambda$) for different off-focus positions and different beam waist sizes w_0. (a): $w_0 = 5\lambda_0$; (b): $w_0 = \lambda_0$.

The findings that the spectral shape does not change significantly with respect to the particle location in both off-center and off-focus directions for reasonably focused beams (beam waist size larger than $5\lambda_0$) is very important for practical SOCT measurements. This implies that the SOCT wavelength-dependent scattering measurement error, for this case, arises mostly from various optical aberrations, which are relatively easy to correct or estimate. Therefore, it is possible to perform wavelength-dependent scattering analysis in this case without precisely knowing the locations of the scatterers in the beam. For a very tightly focused beam, the error may be caused by the oblique components of Gaussian beams. This error usually is very difficult to correct or estimate due to the uncertain nature of the scatterer position and the complexity of the scattering theory.

3.2. Effect of multiple scatterers in the imaging volume

For this analysis, the Gaussian beam, digitization method, sphere sizes, and refractive indices were identical to those used in the previous section (3.1) with a beam waist size $w_0 = 5\lambda_0$. The time window used in SOCT time-frequency analysis was assumed to be a box function of length corresponding to 10 coherence lengths. The spheres were assumed to be randomly located inside the imaging volume defined by the Gaussian beam and the time-window following a uniform distribution. Dynamic focusing was assumed such that the imaging volume was exactly at the waist of the beam. Any sphere that was partially inside the image volume was counted as a whole sphere.

Figure 5 shows the simulated wavelength-dependent scattering patterns produced with multiple spheres in the imaging volume for both sphere sizes. As expected from Eq.(13), there is a significant amount of spectral modulation that corrupts the oscillation patterns predicted for the scattering of a single incident plane wave by a single sphere.

#7680 - $15.00 USD Received 2 June 2005; revised 26 June 2005; accepted 29 June 2005

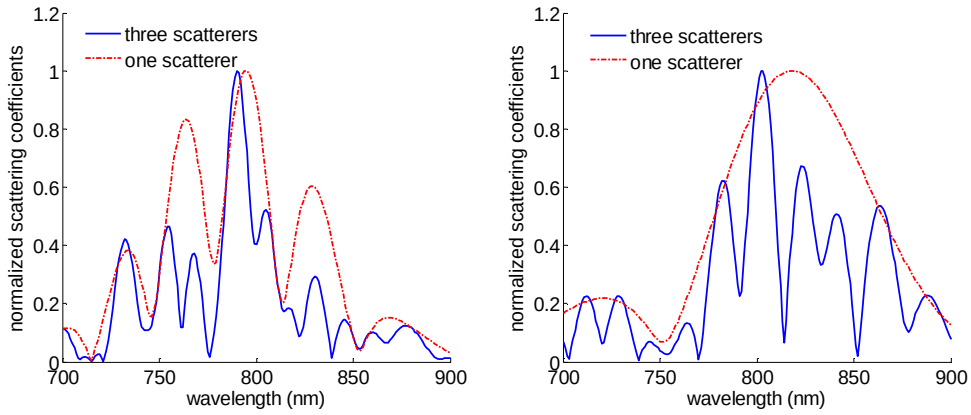

Fig. 5. Examples of spectral modulation patterns due to multiple scatterers (three scatterers here) in the imaging volume for (a) large spheres ($r = 5\lambda$) and (b) small spheres ($r = \lambda$). In each case, the incident laser beam waist size was $w_0 = 5\lambda_0$.

In Fig. 5, it is assumed that the two homogeneous samples contain the same number of large or small scatterers. This implies a much lower volume density for samples with small scatterers. A more common scenario in SOCT experiments is when the volume densities of scatterers are similar. Fig. 6 shows the simulated spectral scattering patterns for spheres with a fixed volume density of 10%. If the scatterer size is large, most likely there is only one scatterer in the imaging volume. However, if the scatterer size is small, there will be multiple scatterers in the imaging volume. As seen from Fig. 6, it can be extremely difficult to distinguish the wavelength-dependent scattering pattern of a large scatterer from the pattern of multiple smaller scatterers based on only one SOCT measurement, as observed experimentally [25].

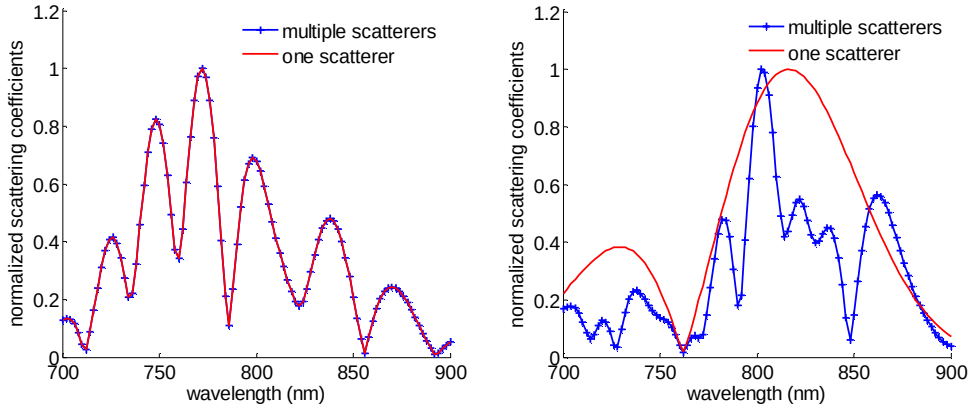

Fig. 6. Examples of spectral modulation patterns due to multiple scatterers of the same volume density (10%) for spheres of radius (a) 5 μm (N<1), and (b) 1 μm. In each case, the incident laser beam waist size was $w_0 = 5\lambda_0$ and the scatterer radius was λ_0 .

#7680 - $15.00 USD
Received 2 June 2005; revised 26 June 2005; accepted 29 June 2005

In many cases, the tissue demonstrates layered or regional structure where adjacent scatterers (either in axial or transverse directions) are more or less homogeneous. As seen from Figs. 2-4, if weak focusing (low NA) is used, the actual single-scatterer spectral scattering can be resolved by extensive incoherent averaging. Although OCT is typically referred to as a coherent high-spatial resolution imaging method, there are several occasions when incoherent averaging is possible over adjacent scan lines. Incoherent averaging is also possible by utilizing many so-called "diversity" methods used in OCT speckle-reduction, *e.g.*, polarization or angular diversity [26]. Fig. 7 demonstrates how the averaged results approach the single-scatterer response. The mean-square error of averaged scattering spectra from the scattering spectrum of a single-scatterer reduces with respect to the number of incoherent averaging according to the formula

$$Error = kN^{-1/2}, \tag{14}$$

where k is the proportional constant and *N* is the number of incoherent averaging.

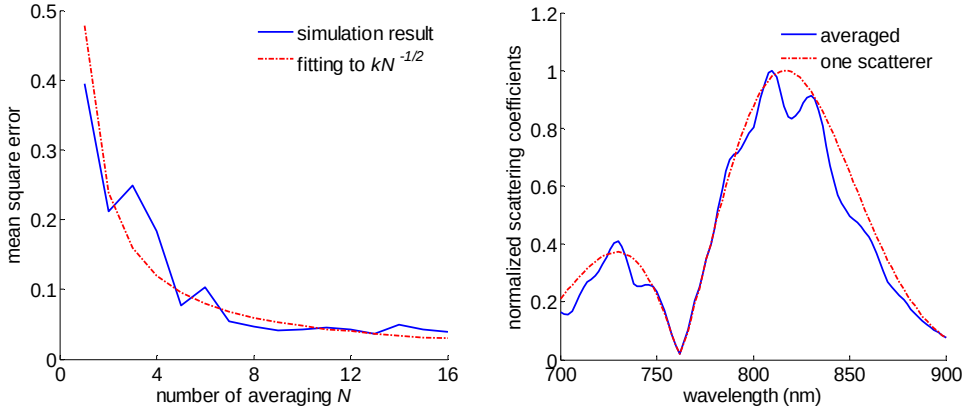

(a) (b)

Fig. 7. (a) Reduction of spectral modulation by incoherent averaging. (b) Examples of spectral modulation patterns after incoherent averaging (three scatterers with N = 16). The incident laser beam waist size was $w_0 = 5\lambda_0$ and the scatterer radius was λ_0 .

Perhaps the most common SOCT scenario in biological imaging is that of one large scatterer surrounded by several small scatterers. For example, cells may have only one nucleus, but may have several mitochondria and multiple other small scatterers. It is often desirable to resolve the wavelength-dependent scattering due to the large scatterer in the presence of these smaller scatterers. We found that for many cases, the spectrum measured by SOCT in this scenario depends on the exact location of the large scatterer within the imaging beam. Fig. 8 shows the simulation of the spectral scattering for the case of one large scatterer surrounded by a number of randomly placed small scatterers.

#7680 - $15.00 USD Received 2 June 2005; revised 26 June 2005; accepted 29 June 2005

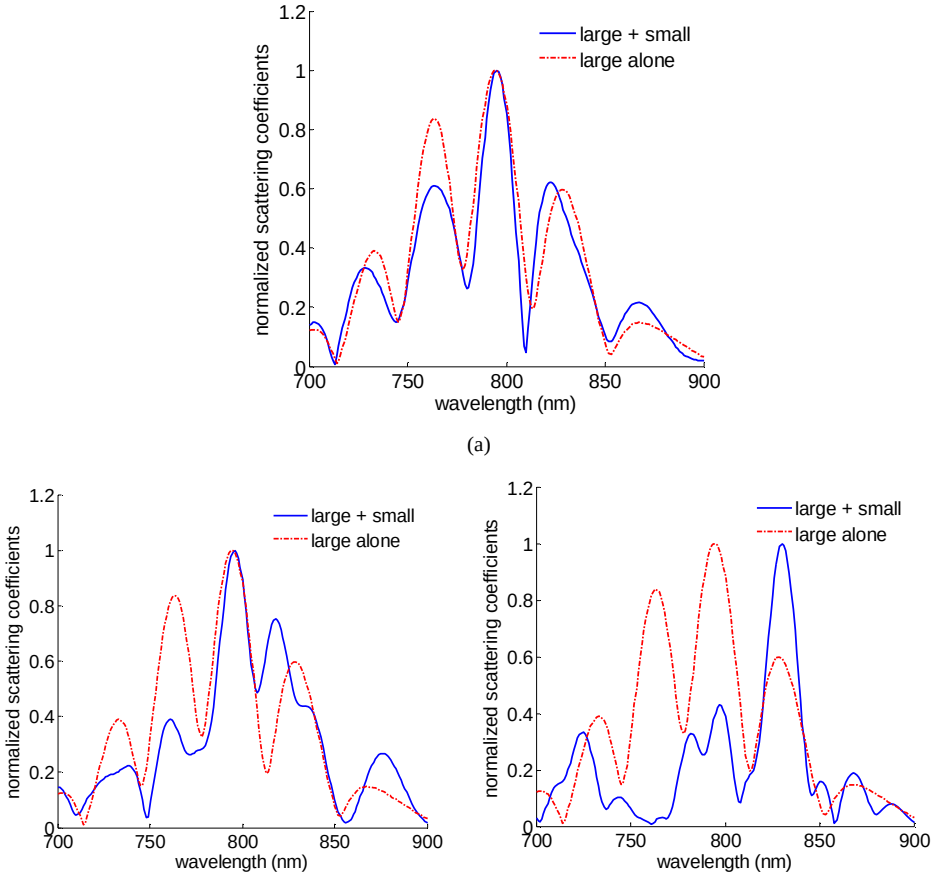

Fig. 8. Examples of spectral modulation patterns for a large scatterer ($radius = 5\lambda_0$) surrounded by many small scatterers ($radius = \lambda_0$): (a) when the large scatterer is at the center of the beam; (b) when the large scatterer is off-center by u_0 ; (c) when the large scatterer is off-center by $2u_0$. The number of smaller scatterers was chosen such that they occupied the same total volume as the large scatterer.

Fig. 8 shows that when the volume density of a large scatterer and small scatterers are similar, the overall spectral scattering depends on the exact location of the large scatterer within the Gaussian beam. If the large scatterer is in the center of the beam, the scattering is dominated by the larger scatterer. When the large scatterer is gradually moved off-center from the central region of the Gaussian beam, the scattering profile for the large scatterer is gradually corrupted by the modulation effect due to the presence of the small scatterers. This means that in some cases, the scattering due to the large scatterer can be resolved by over-sampling the SOCT signal while transverse scanning, followed by a computational search for the signal maximum.

4. Discussion

Previously, SOCT has been used for imaging changes in absorption. However, absorption-mode SOCT imaging suffers from a concentration-pathlength tradeoff. For an absorber to significantly shift the spectrum of the back-scattered light, Beer's law dictates that the absorber either needs to be present in high concentration or the length of the absorber region

#7680 - $15.00 USD Received 2 June 2005; revised 26 June 2005; accepted 29 June 2005

must be large. Both are difficult to achieve *in vivo* since OCT is a high-resolution imaging method and few biological molecules are absorbing in the near-infrared. The scattering-mode SOCT described here does not suffer from this tradeoff since the spectral shift in scattering is almost a point effect. In addition, because absorption-mode SOCT is often designed to attenuate certain wavelength bands, the spectrum propagating to deeper structures often is different from the laser spectrum incident on the surface, producing a "spectral shadowing" effect. On the other hand, in scattering-mode SOCT, although each scatterer may act as a Mie scatterer that attenuates the light, the forward scattering and the ensemble effect exhibit linear or flat attenuation across the laser spectrum [22]. From these two points, it is expected that scattering-mode SOCT can potentially yield a more sensitive and localized signal than absorption-mode SOCT.

The difficulty associated with measuring the scattering-mode SOCT includes the various effects discussed in this paper, and the complexity of the data-processing algorithm. The inhomogeneous properties of tissue scatterers, such as variations in size, refractive index, and density, make the wavelength-dependent scattering measurement a challenge to interpret. In addition, Mie theory is significantly more complicated and more numerically complex than Beer's law. These challenges may account for why scattering-mode SOCT, although an intuitive approach, was only recently investigated to enhance OCT contrast [25].

For interpretational and computational simplicity, the scalar scattering theory was used in these simulations for calculating the field scattered off spheres. Implementing algorithms based on scalar scattering theory is straightforward and the computational burden is minimal. Because the polarization state in a fiber-based OCT system can be difficult to model, and varies between systems, we have focused on obtaining qualitative results in this initial work. Vector scattering models with polarization consideration, which are currently being developed in our group, will provide more accurate results when the polarization of the OCT system can be modeled accurately.

In this paper, we have demonstrated the potential of using SOCT to accurately match the wavelength-dependent SOCT scattering measurement to those calculated based on plane waves for two specific situations. First, when the scatterers are relatively homogeneous in a region, incoherent averaging can be used to reduce the modulation effect. Second, when there is only one dominant scatterer in the imaging volume, accurate matching to wavelength-dependent scattering can be retrieved by spatially over-sampling and analyzing the spectrum corresponding to the maximum scattering point. However, with the development of new spectral analysis algorithms, measurements of spectral scattering for other situations should also be possible. New spectral analysis algorithms will be more accurate in a practical implementation if phase stability in the imaging system can be achieved, *e.g.*, by using a well-characterized spectral-domain OCT system. In this case, the interferometer can be characterized using the linear equation Eq. (10) instead of Eq. (11). Implemented in this manner, it should be possible to jointly estimate the positions and properties of the scatterers using only one or a few axial (depth) scan lines. The use of scattering-mode SOCT algorithms has the potential to further improve our ability to extract biologically- and medically-useful information from tissue for diseases such as cancer, where changes in nuclei and cell size have diagnostic significance.

Acknowledgments

We gratefully acknowledge the helpful discussions with Yuan Liu, Yang Liu, and Daniel Marks. This work was supported in part by the National Institutes of Health (NIBIB, 1 R01 EB00108, S.A.B.), the National Science Foundation (BES 0347747, S.A.B.; 0239265, P.S.C), and the UIUC-UIC Intercampus Research Initiative in Biotechnology (S.A.B.).

#7680 - $15.00 USD Received 2 June 2005; revised 26 June 2005; accepted 29 June 2005